

FIFTH INTERNATIONAL CONGRESS ON SOUND AND VIBRATION

DECEMBER 15-18, 1997
ADELAIDE, SOUTH AUSTRALIA

THE EFFECTIVENESS OF SPARSE RANDOM ARRAYS FOR UNDERWATER ACOUSTIC IMAGING

David G. Blair, Jim Thompson and Stuart Anstee

Maritime Operations Division, Defence Science and Technology Organisation,
PO Box 44, Pyrmont, NSW 2009

It is intended to produce an underwater acoustic imaging system with three-dimensional images of resolution around 1 mm at 1 m range. For this purpose, sparse random arrays have considerable cost and feasibility advantages over filled arrays. There is no degradation of beamwidth, while the average distant sidelobe level (ADSL) can be reduced to a level expected to be satisfactory for imaging surfaces such as sea mines, although unsatisfactory for imaging continua such as human tissue.

We have simulated the imaging of point targets by random arrays of N elements. The simulation uses exact path lengths in the near field. Good range resolution is obtained through either a short toneburst or a cross-correlated chirped signal. It is confirmed that, as the array is made more sparse, the ADSL rises. For broadband signals, the ADSL is found to be markedly lower than the monofrequency value. The use of partially random arrays, constructed out of identical subarrays for ease of manufacture but oriented randomly, leads to an appreciable degradation in ADSL. For example, a system of 100 square subarrays with four subarray orientations resulted in an ADSL penalty of 5 dB.

1. INTRODUCTION; THE RANDOM ARRAY

DSTO, along with its industrial partners, Thomson Marconi Sonar and CSIRO, is working to produce an underwater acoustic camera which would yield three-dimensional (3-D) images having an angular and range resolution of 1 mm per m of range. It is intended to use a broadband correlated chirp, centred on a frequency of roughly 3 MHz, a broad-beam omnidirectional transmitter and a *sparse, random planar* receiving array. 'Sparse' here means sparse compared to a 'filled' array, the latter being a regular array with just sufficient elements to avoid grating lobes. A filled *square* array has an element spacing of $\lambda / 2$, where λ is the central wavelength. Theoretical results confirmed by experiment (Steinberg 1976, Steinberg and Subbaram 1991) show that, despite its sparseness, such an array performs surprisingly well. The beamwidth of the sparse array depends almost entirely on the overall

aperture and is practically the same as for the filled array. The penalty for using a sparse array consists in a raised value of the average distant sidelobe level (ADSL) which, for a monofrequency (continuous-wave—cw) signal, is independent of angular displacement and equal to $1/N$, where N is the number of elements. The distant sidelobes derive their importance as follows: for a given voxel, all the scatterers at the same range as that voxel, including those at a large angular displacement from it, make a contribution to that voxel through the sidelobes. The contributions from the distant lobes combine to give a background fog or ‘clutter.’

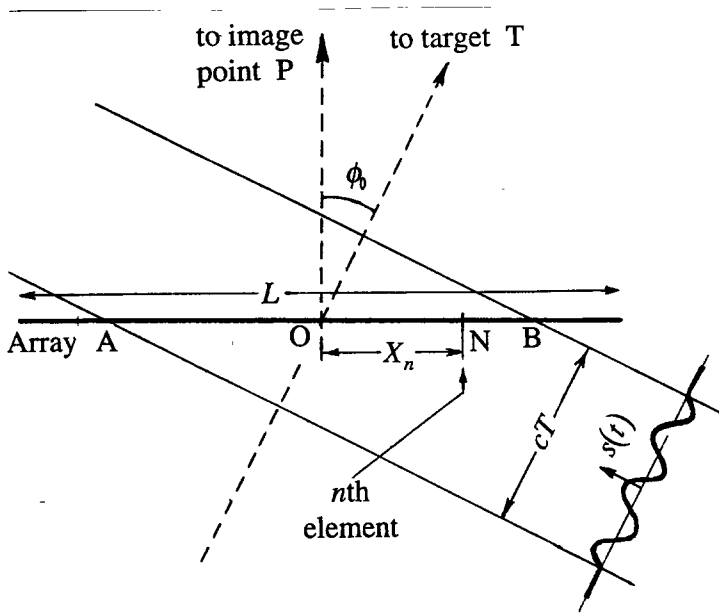


Figure 1. Only elements from A to B contribute to the image at P. Shown here is the reciprocal configuration to the one normally of interest.

For imaging targets such as sea mines, in which the scattering of ultrasound is overwhelmingly from *surfaces*, analyses have concluded that the ADSL can be reduced to a satisfactory level by increasing the number of elements N to a moderate value (say 3000 to 4000). The analysis involves noting that, given any voxel, *the troublesome scatterers* contributing to the intensity of that voxel lie on the curve of intersection of the mine surface with the surface of the sphere centred on the array centre and passing through the voxel. The number of troublesome scatterers can be estimated and can be compensated for by making N large enough.

On the other hand, for medical imaging, it is not expected that a random array with the same high degree of sparseness would be satisfactory, for the following reason. In tissue, the scatterers are spread throughout a *volume*. The intersection with the spherical surface is now that surface itself. Since the intersection is a surface, not a curve, the number of troublesome scatterers becomes much larger.

We have developed a computer program, POINTSPR, to assist in the design of the array system. The program handles a wide variety of planar arrays, using near-field beamforming to produce either 2-D or 1-D slices through the 3-D image.

2. BEAMFORMING

For later use, we give here the essential equations for beamforming and give also a graphical method useful in understanding some properties.

If an active sonar array with an omnidirectional point transmitter insonifies a region containing point scatterers, then the voltage at the n th sensor element of the array is

$$E_n(t) = \sum_j \frac{a_j}{\rho_{j_i} \rho_{j_n}} s[t - c^{-1}(\rho_{j_i} + \rho_{j_n})] \quad (1)$$

Here a_j is the scattering strength of the j th point scatterer, ρ_{j_i} and ρ_{j_n} are the distance of that scatterer from the transmitter and n th element respectively, $s(t)$ is the transmitted pulse,

taken to be centred on $t=0$, c is the sound speed, and constant factors in $E_n(t)$ have been omitted. Our simulations assume an array of elements in the xy plane, a single point scatterer, a point transmitter at the origin and a pulse s that is either a short toneburst or a correlated, rectangular-envelope, linear chirp. Beamforming appropriate to a short toneburst is performed thus:

$$A(\mathbf{r}) = \sum_n w_n E_n \left[c^{-1} (\rho_{r_t} + \rho_{r_n}) \right] \quad (2)$$

(Knudsen 1989). Here $A(\mathbf{r})$ is the 'radio-frequency' image amplitude at the position \mathbf{r} (the 'image point'), the w_n are shading weights, and ρ_{r_t} and ρ_{r_n} are the distance of \mathbf{r} from the transmitter and the n th element respectively. The total image amplitude $A_t(\mathbf{r})$ is essentially an envelope of $A(\mathbf{r})$. Crosscorrelation or dechirping is described by Rihaczek (1985). The dechirped response can be calculated by replacing $s(t)$ by its autocorrelation function.

Simulations below for short and effectively short pulses yield novel results. An approximate but easily-understood explanation of some of these results is derived as follows. First, the incoming spherical waves from a scatterer are nearly plane if the range of the scatterer is greater than about L^2/λ , where L is the aperture size (the length in the case of a square or linear array). For simplicity we assume the scatterer to be at such a range; that is, to be in the 'far field' of the array (Steinberg 1976). Then for an unweighted array ($w_n=1$), omitting the slowly-varying factors that precede s in Eqn (1), we have

$$A(\mathbf{r}) \approx \sum_n s \left\{ c^{-1} \left[2(r - r_0) - X_n (\sin \phi - \sin \phi_0) \right] \right\} \quad (3)$$

For ease of presentation we consider here a linear array along the x axis, X_n is the n th element position and ϕ is the angle that the vector \mathbf{r} to the image point P, lying in the xz plane, makes with the z direction (broadside). The subscript 0 refers to the single target at T. We now consider the case $\phi=0$, i.e. the image point is held fixed at $\phi=0$ while the target's position is varied. This is the *reciprocal* configuration to what normally interests us (target fixed, image point varying); but it is well known that the two intensity beam patterns the result are the same. Then for a pulse of duration T , the n th element will contribute only if

$$-T/2 < c^{-1} \left[2(r - r_0) + X_n \sin \phi_0 \right] < T/2 \quad (4)$$

That is (Fig. 1), the element must lie in the slice between two parallel planes. These planes actually represent the beginning and end of the pulse that was transmitted and then scattered from the target, the wavefronts in the neighbourhood of the array being approximately plane. We consider the transverse beam pattern (P and T at the same range) by putting $r=r_0$ in (4); this makes the centre of the slice pass through the origin. Clearly *some elements of the array fail to contribute if*

$$\left| c^{-1} (L/2) \sin \phi_0 \right| > T/2, \quad \text{i.e.} \quad \left| L \sin \phi_0 \right| > cT \quad (5)$$

The normal, i.e. nonreciprocal situation (target fixed at $\phi_0=0$) is represented in Fig. 1 by interchanging P and T and replacing ϕ_0 by ϕ . Regarding results, the normal situation is described by *replacing ϕ_0 by $-\phi$* in (4) and (5) (or equivalently, by $+\phi$ in Eqn 5). From now on we shall consider this done.

The above results are easily generalised to a planar array (xy plane). Provided that the target and image point are in the xz plane, Eqn (3) holds. The array is effectively projected onto the x axis. Likewise (4) holds. In (5), L must be interpreted as the length of the array after projection onto the x axis; it is of course the ordinary length in the case of a square array with sides in the x and y directions.

3. SIMULATION RESULTS AND DERIVATIONS FOR RANDOM ARRAYS

A number of graphs giving results of simulations for random arrays will be shown in the oral presentation. The written paper concentrates on theoretical explanations of some of those results, so that the presentation can treat the derivations lightly.

The simulations for this section use the following parameters, except where otherwise stated:

pulse: central frequency $f_c = 3.5$ MHz ($\lambda = 0.43$ mm); either a short toneburst (duration T roughly equal to $4/f_c$) or a correlated chirp (bandwidth B roughly 1 MHz)

array: square; random, 3200 elements (on average); aperture 430 mm (1000λ)

point target: at 1 m range, at broadside

image slice: 1-D, through target, along arc in xz plane

These parameters lead to a transverse resolution of 1mm per m of range, and a range resolution of approximately 1 mm—the same values as called for in the mine imaging system.

The simulations show, first, that for signals that are short, or effectively short (short after dechirping), the ADSL is consistently below the monofrequency level $1/N$. Furthermore the level decreases with increasing angle ϕ . These results are explained as follows. Consider a random square array with $\phi_0 = 0$ and ϕ in the xz plane as just described. For a *short toneburst*, under condition (5), the fraction of elements contributing is $cT / L \sin \phi$, so the number contributing is $N_c = N(cT / L \sin \phi)$. For the purpose of comparing peak and sidelobe, we may regard each element as receiving a signal of unit strength. At the peak, all signals are combined coherently, giving an image amplitude of N and an intensity of $I_0 = N^2$. In the sidelobes, the signals add incoherently, so the intensities add, yielding $I = N_c$. The *average distant sidelobe level* (ADSL), measured as intensity relative to the peak, is then

$$\text{ADSL} = I/I_0 = N_c / N^2 = cT / (NL \sin \phi) \quad (6)$$

Note that, since this value depends on ϕ , it is a *local* value, the average being over the ensemble of arrays. Note also that in the cw case, the above argument would yield $I = N$ and hence, in place of (6), the well-known result $\text{ADSL} = 1/N$ (Steinberg 1976).

For a *correlated chirp* of bandwidth B , a corresponding calculation can be performed. Now the intensity response of an element is proportional to the square of the autocorrelation function of $s(t)$ rather than to the (squared) rectangular window of $s(t)$ itself. The resulting expression for the sidelobe level can be simplified under the condition $c/B \ll L|\sin \phi|$. [Note the sign \ll , as opposed to the simple $<$ or $>$ that was present in the short burst case (5).] Then the result is

$$\text{ADSL} = c / (NBL \sin \phi) \quad (7)$$

Comparing (7) with (6), we see that, for sufficiently distant angles, the chirp is *equivalent* to a short burst of length T_e , where $T_e = 1/B$.

The predicted results (6) and (7) are compared, in Fig. 2, with two simulations: a toneburst of 4 cycles duration and a chirp with bandwidth $B = f_c/4$. Note that the two are equivalent in the sense just defined. Also shown is the beam pattern for a long toneburst (for which the ADSL is $1/N$). To obtain better statistics, for each angle, an average of the simulated intensity over 50 arrays (Monte Carlo calculation) is taken. The three horizontal lines traversing the page are the respective computed average sidelobe levels (CASL). Here and below, the CASL is calculated as the average over all positive angles ϕ shown, but omitting the 25% of angles nearest the peak (at $\phi = 0$). (Here 'arc' may be substituted for

‘angle’). Note that in the present case the CASL is an average over both arrays and angles. $\Delta\theta$ is the angular interval $0 < \sin\phi < cT/L$ (Eqn 5) for which the formula (6) for a short toneburst does not apply. The crosses are points predicted by *both* Eqn (6) (short toneburst) and Eqn (7) (chirp). The results are seen to agree well with the prediction. The chirp result is claimed above as valid only if $\sin\phi \gg c/BL$, but interestingly, the chirp is found to fit the formula well subject only to the condition $\sin\phi > c/BL$. The figure also shows (short horizontal line) the predicted CASL. The small discrepancy for the short toneburst corresponds to a factor of 1.12 in intensity. This discrepancy appears to be accounted for statistically by the fact that only 50 arrays were averaged.

A second area of simulations involves the use of *partially* random arrays, constructed out of identical subarrays, or ‘tiles’, for ease of manufacture. One simulation compares the fully random array with an array constructed from 100 identical tiles, arranged as 10×10 , each tile being oriented randomly among four orientations. For the particular parameters used (0.08% of filled-array sites occupied, chirp, $B=1$ MHz), the beam patterns resulting after averaging over 400 arrays are shown in Fig. 3. The figure shows that changing to the replicated tile causes the sidelobe level (CASL) to rise by 5 dB.

While we have been unable to explain the 5 dB value, we have been able to explain approximately the shape of the replicated-tile curve. In an approximation valid when $l \ll T$, the autocorrelation function of the chirp, when the analytic signal (Rihaczek 1985) is used to represent the latter, becomes

$$Y_a(t) = \text{sinc}(Bt) \exp(j2\pi f_c t) \quad (8)$$

(subscript a for analytic), where $\text{sinc } x = \sin(\pi x) / \pi x$. The Fourier transform of $Y_a(t)$ is

$$Y_a(f) = \int_{-\infty}^{\infty} Y_a(t) e^{-j2\pi ft} dt = B^{-1} \text{rect}[B^{-1}(f - f_c)] \quad (9)$$

where $\text{rect}(x)$ is 1 for $|x| < 1/2$ and is 0 elsewhere.

Consider separately the Fourier component for each f . Because the tiles in any two positions are identical, even in orientation, one quarter of the time, we expect grating lobes to occur, giving rise to increased sidelobe intensity. They will occur when

$$k_e L_t = n2\pi, \quad \text{with} \quad k_e = 2\pi / \lambda_e, \quad \lambda_e = \lambda / \sin\phi \quad (10)$$

Here L_t is the length of a tile, n is an integer, λ_e is the effective wavelength along the x axis and $\lambda = c/f$. Thus grating lobes should occur at

$$\sin\phi = nc / L_t f \quad (11)$$

But we have seen in Eqn (9) that the spectrum of $Y_a(t)$ is rectangular, with the end-points $f_c \pm B/2$. Therefore the intensity should be enhanced in the interval

$$nc/L_t (f_c + B/2) < \sin\phi < nc/L_t (f_c - B/2) \quad (12)$$

for each $n = 1, 2, 3, \dots$

Comparison with Fig. 3 shows first, that a series of peaks does occur and that their shapes, beyond the first side peak (around azimuth arc 10 mm), bear a striking resemblance to a rectangle. Second, the calculated intervals (12) for enhanced intensity are each shown in the figure as a pair of vertical lines joined by a broken horizontal line to aid the eye. Up to where comparison becomes impossible, the values are in fairly good agreement with the positions at which the computed intensity rises sharply and falls sharply. (Comparison becomes impossible when the $n=5$ peak begins, because that peak overlaps the $n=4$ peak.)

Image Intensity along Arc

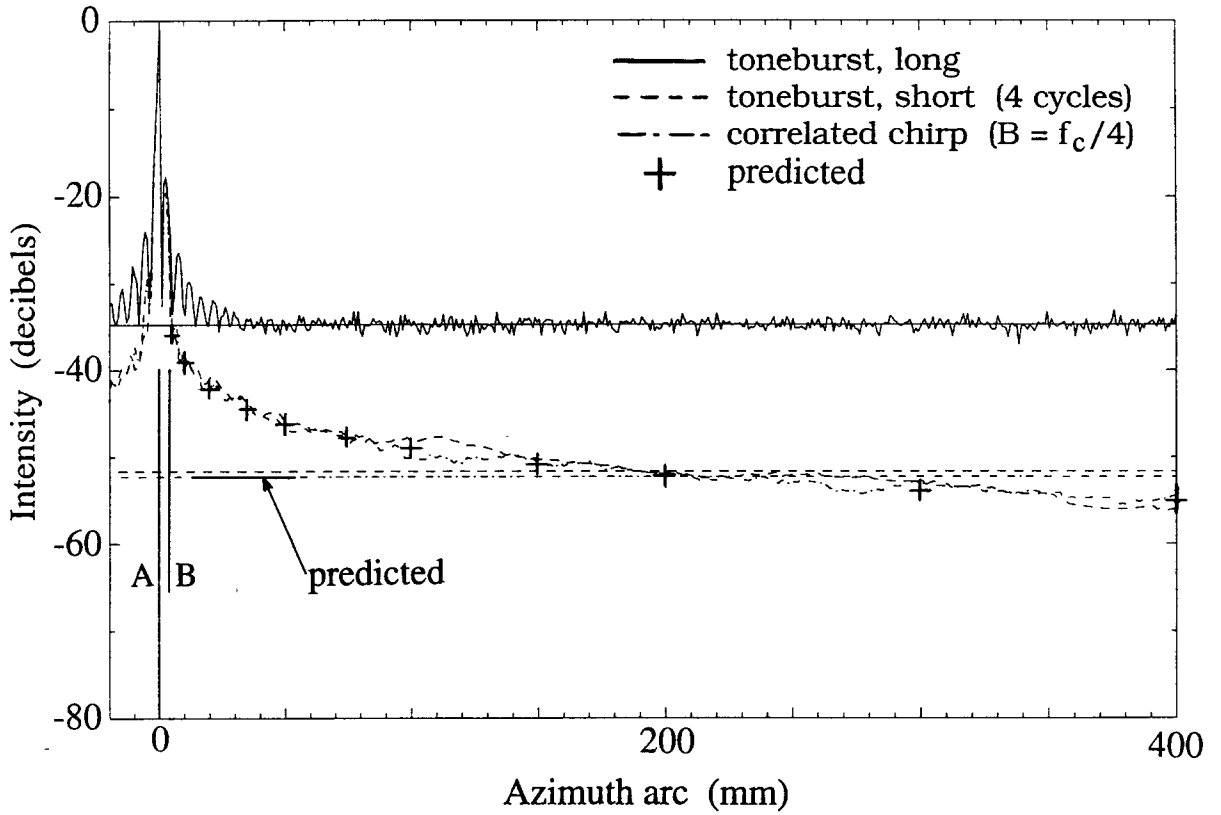


Figure 2. Sidelobe averages for a short toneburst and a correlated chirp.

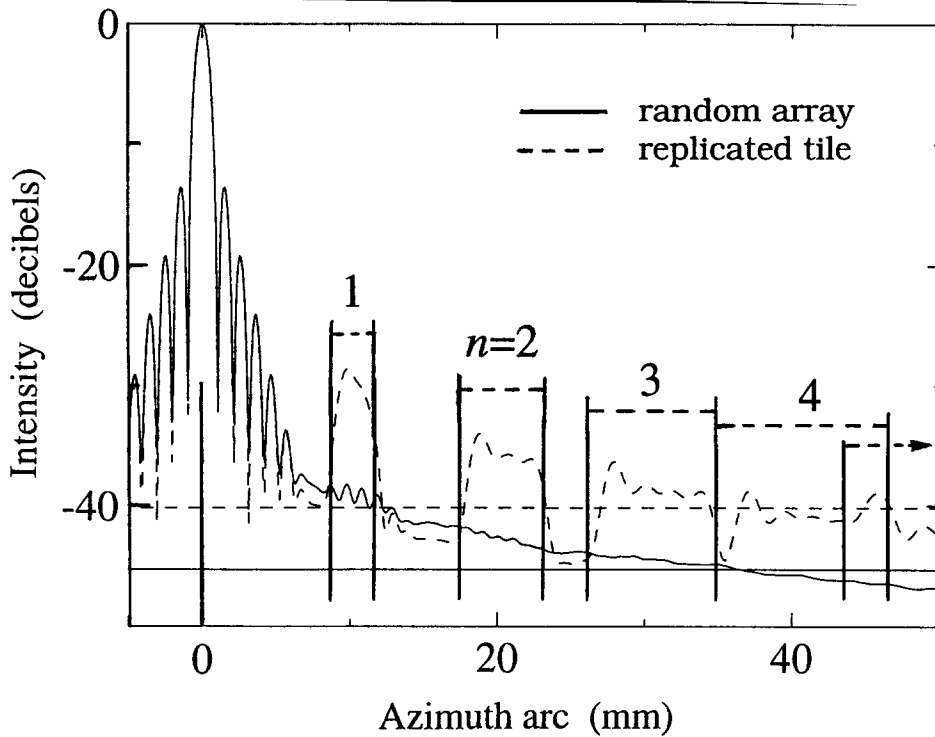


Figure 3. Replicated tile compared to a truly random array

4. VARIATION OF BEAM PATTERN WITH SPARSENESS

We have simulated the effect of increasing sparseness by considering a square array which, when filled, has 40 000 elements with a spacing of half a wavelength. This array was chosen because, when thinned to $N=32$ elements, it is the same as a tile being considered for the acoustic mine imaging array, the array being formed from 10×10 tiles. Furthermore it may be that a single tile will often be used on its own, to obtain a lower-resolution image, the advantage being that a vastly reduced amount of signal processing would be required.

In detail, the simulations in this section use the following parameters:

pulse: short toneburst, central frequency $f_c = 3.5$ MHz ($\lambda = 0.43$ mm), duration=4 cycles

array: square; aperture 43 mm (100λ); random, 40 000 to 16 elements

point target: at 10 m range, at broadside

image slice: 1-D, through target, along a great circle

The image was calculated on a sphere at the range of the target, but only on some great circles of the sphere. The main calculations were done for a great circle in the xz plane (plane parallel to one side of the square array).

As the number of elements N was decreased from 40 000 to 16, through seven values of N , the changing beam pattern was calculated (figures to be presented) and several of its parameters were monitored. It was found that, first, the 3 dB beamwidth hardly changes with decreasing N ; even at $N=16$ it has risen only by 10%. Second, as shown in Fig. 4, the heights of the two inner sidelobes remain constant down to about $N=50$. Third (Fig. 4), the computed average sidelobe level, relative to the peak, is given approximately by $CASL=0.22/N$. This formula is to be compared with the expression $1/N$ for the monofrequency (cw) case: evidently the short pulse yields a reduction in sidelobe level and hence an improvement. The result $CASL=0.22/N$ is explained roughly by the theoretical formula (6) obtained above. That formula, averaged over the relevant angles, actually yields $CASL=0.186/N$. The agreement is regarded as satisfactory, since only one array was used at each degree of sparseness, yielding a considerable statistical error.

The beam pattern for the filled array has a peculiar shape, in which the level becomes very low from the 4th 'node' onward (i.e. from the end of the third sidelobe). By way of explanation, the criterion $L \sin \phi = cT$ (Eqn. 5) holds at this point. So from Fig. 1 (reciprocal system), at larger angles only a subset of elements contributes, namely those lying in a slice of width 4λ , measured perpendicular to the wave front. Because there are very many elements—almost a uniform continuous distribution—and because as we proceed across the slice the phase of the voltage changes by a whole number of cycles (four), the voltages when added yield almost the integral of a sine curve over exactly four cycles. The latter is zero; hence the very low level.

The beam pattern for the larger and medium values of N is very jagged: a sudden jump in the curve of intensity versus angular displacement ϕ occurs at many values of ϕ . These jumps are explained by Eqn (5) and the subsequent discussion of planar arrays. Each row of elements pointing in the y direction behaves as though it were projected onto the middle point of that row. Hence, as ϕ increases, a *whole row* of elements having coordinate x stops contributing at the value of ϕ given by $2|x|\sin \phi = cT$; hence the jump. And the process is repeated with each row. We present results for an image slice along a second great circle, through the target but intersecting the first circle at an angle of 35° . It is found that the beam pattern becomes less jagged, as expected.

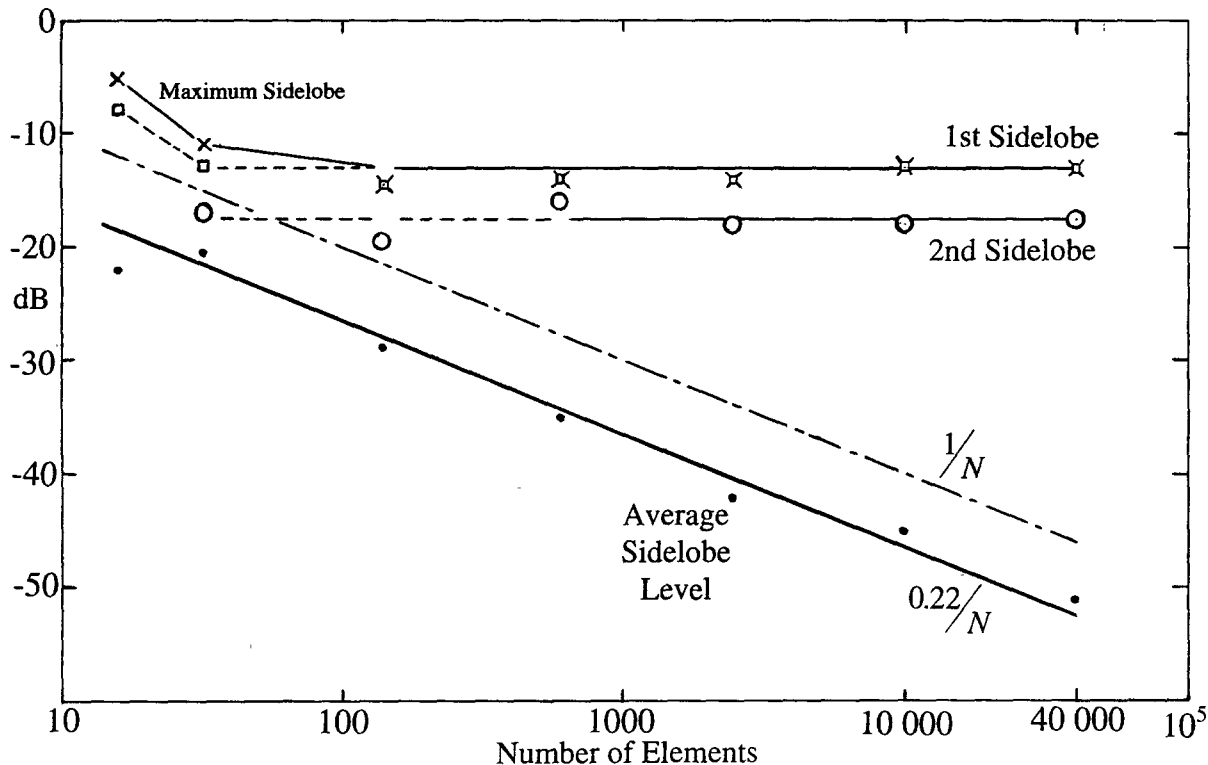


Figure 4. Performance of sparse random arrays.

5. CONCLUSION

We have performed a number of simulations and provided analytical arguments. These support the conclusion that the random array should be very useful in acoustics under suitable conditions. The usefulness is increased when the array is two-dimensional, the number of elements in the filled array is extremely large, the object to be imaged is a surface, and a short or effectively short pulse is used.

6. ACKNOWLEDGEMENTS

Dr Ian S.F. Jones made a number of useful suggestions.

7. REFERENCES

- Knudsen, D.C. (1989). A New Beamformer for Acoustic Imaging. In: *Oceans '89: An international conference addressing methods for understanding the global ocean*. New York: IEEE Press.
- Rihaczek, A.W. (1985). *Principles of High-Resolution Radar*, Revised Version. Los Altos, Calif.: Peninsula.
- Steinberg, B.D. (1976). *Principles of Aperture and Array System Design—Including Random and Adaptive Arrays*. New York: John Wiley.
- Steinberg, B.D. and Subbaram, H.M. (1991). *Microwave Imaging Techniques*. New York: John Wiley.